Eigenchannel quantum-defect theory of open-shell atoms. II. Calculation of $3p^4(^3P)ns$ Rydberg spectra of the chlorine atom

Z.-w. Wang* and K. T. Lu†
Argonne National Laboratory, Argonne, Illinois 60439
(Received 9 April 1984)

Rydberg spectra of the chlorine atom $3s^23p^4(^3P)ns$, $J=\frac{1}{2}$, $\frac{3}{2}$, and $\frac{5}{2}$, are calculated by use of an eigenchannel quantum-defect method. The results indicate that the channel interactions due to electrostatic and spin-orbit potentials are weak. The effect due to channel interaction of the $3s\,3p^6$ configuration is completely negligible. Agreement with emission data is excellent ($\lesssim 0.2\%$ accuracy except for the lowest $n=4$ levels). Autoionization resonances are predicted.

I. INTRODUCTION

Rydberg spectra for open-shell atoms have long been recognized as a challenging problem for both theoretical and experimental work. Recently, we have begun to disentangle the chlorine spectra[1] seen in the photoionization cross section[2] and in early discrete emission data.[3] Specifically, we have introduced[1] the "effective channel" in connection with the time-delay matrix suitable for analyzing autoionization resonances. In the present paper we report a calculation of Rydberg levels of the chlorine atom in terms of quantum-defect parameters, namely, eigen-quantum-defect μ_α and channel-mixing angles θ. We aim at establishing the connections between a configuration-mixing treatment and an eigenchannel quantum-defect theory (EQDT).[4,5]

EQDT has evolved into a unified theory of spectroscopy and collision processes in atoms[5] and molecules.[6] This unification is achieved by treating eigenchannel phase shifts and time-delay matrix in terms of basic quantum-defect parameters.[1] Thus, it permits the extraction of collisional information from the wealth of spectroscopic data. *Ab initio* calculations of quantum-defect parameters have also been made.[7–9]

On the other hand, configuration-mixing calculations of atomic[4,10] and molecular[11] wave functions by variational techniques, via trial electronic wave functions, have been very successful for low-lying states. However, in calculating highly excited or continuum states, one encounters several difficulties. The large number of required configurations, the poor orthogonality between states of the same symmetry, and the poor numerical convergence are major problems. The many-body dynamics for open-shell atoms and the necessity of including several configurations in the ground-state wave function make these problems especially intractable.[12–14]

In this paper we use the Hartree-Fock program of Froese Fischer[10] to calculate these EQDT parameters for $3p^4(^3P)ns$ Rydberg series of the chlorine atom. Rydberg energy levels and the time delay of the interacting channels can then be evaluated insofar as these EQDT parameters depend weakly on the total energy of the system. This procedure may be useful for molecular systems where experiment has not yet provided information accurate enough to give quantum-defect parameters.

II. THE $3p^4(^3P)ns$ RYDBERG SPECTRA OF THE CHLORINE ATOM

Photoabsorption of a neutral chlorine atom from its ground state, $3p^5(^2P_{3/2})$, leads to $3p^4(^3P)ns$ and $3p^4(^3P)nd$ configurations with $J=\frac{1}{2}$, $\frac{3}{2}$, and $\frac{5}{2}$, and even parity, and thence to 19 series in the final states. The configuration interactions between the ns and the nd series are very weak and can be neglected entirely. We can thus decouple the ns channels from the nd channels and focus on the interacting ns channels only. There are five ns channels, i.e., one series converges to the $3p^4(^3P_0)$ ion-core level and two series converge to $^3P_1$, and two other series converge to the $^3P_2$ ion-core level. Since channels with different total angular momenta J do not interact, these five channels may be divided into three groups: two two-channel problems, $3p^4(^3P_1)ns$ and $3p^4(^3P_0)ns'$ with $J=\frac{1}{2}$ and $3p^4(^3P_2)ns$ and $3p^4(^3P_1)ns'$ with $J=\frac{3}{2}$ and one single-channel problem, $3p^4(^3P_2)ns$ with $J=\frac{5}{2}$. The eigenvalues of these two two-channel problems are characterized by two effective quantum numbers ν_1 and ν_2, which are related to the ionization potentials I_1 and I_2 for each energy level E_n by the relations

$$E_n=I_1-(2\nu_1^2)^{-1}=I_2-(2\nu_2^2)^{-1} \text{ in a.u.} \tag{1}$$

and

$$\nu_1=\nu_2[1-2(I_2-I_1)\nu_2^2]^{-1/2}\ . \tag{2}$$

The two ionization potentials I_1 and I_2 correspond to the ion-core states $3p^4(^3P_{1,0})$ for $J=\frac{1}{2}$ and $3p^4(^3P_{2,1})$ for $J=\frac{3}{2}$, respectively. We also assign to each level E_n a single quantum-defect $\mu=n-\nu_1$, where n is an integer. The eigenvalue problem of the quantum-defect theory[5] requires all levels to lie on a smooth curve of the form

$$\begin{aligned}F(\mu,\nu_2)=&\sin^2\theta\sin[\pi(\mu-\mu_1)]\sin[\pi(\nu_2+\mu_2)]\\&+\cos^2\theta\sin[\pi(\mu-\mu_2)]\sin[\pi(\nu_2+\mu_1)]\\=&0\ .\end{aligned} \tag{3}$$

TABLE I. The values of ζ_{3p}, G^1, and $\nu_1^3 G^1$ for the configuration $3p^4(^3P)ns$ of atomic chlorine, calculated by the use of the HF program.

State	ζ_{3p} (cm^{-1})	G^1 (cm^{-1})	ν_1[a]	$\nu_1^3 G^1$
$3p^4(^3P)4s\,^4P$	626.584	2403.5	1.913	16 824.33
$3p^4(^3P)4s'\,^2P$	629.875	1615.8	1.979	12 526.47
$3p^4(^3P)5s\,^4P$	631.573	561.9	2.938	14 259.89
$3p^4(^3P)5s'\,^2P$	632.189	441.2	2.998	11 890.83
$3p^4(^3P)6s\,^4P$	632.511	223.9	3.946	13 760.29
$3p^4(^3P)6s'\,^2P$	632.739	182.8	4.004	11 737.77
$3p^4(^3P)8s\,^4P$	632.958	63.9	5.951	13 470.06
$3p^4(^3P)8s'\,^2P$	633.02	53.7	6.009	11 649.84
$3p^4(^3P)10s$	633.060	26.6	7.953	13 381.37
$3p^4(^3P)10s'$	633.089	22.6	8.010	11 615.54
$3p^4(^3P)12s$	633.101	13.5	9.954	13 314.24
$3p^4(^3P)12s'$	633.111	11.6	10.011	11 637.35
$3p^4(^3P)14s$	633.113	7.8	11.954	13 322.79
$3p^4(^3P)14s'$	633.122	6.7	12.011	11 609.29

[a] ν_1 is the effective quantum number.

Here $\mu_\alpha, \alpha=1,2$ are the eigen quantum defect and θ_α is the mixing angle between these two channels. They correspond to the eigenvalues and eigenvectors, $U_{i\alpha}$, of the reaction matrix which measures the short-range non-Coulombic interactions between the electron and the ion core. The orthogonal matrix $U_{i\alpha}$ transforms the dissociating channel i in which an electron and the ion are loosely coupled by electrostatic interaction to the reactive channel α in which an electron and the ion are strongly coupled by electrostatic interactions (i.e., many-body interactions). For two-channel interactions the frame transformation matrix $U_{i\alpha}$ has only one independent element and can be represented by a mixing angle θ. The quantum defect μ is treated as a continuous variable of energy. Equation (3) determines the functional dependence of μ on the quantum number ν_2 which is a dimensionless quantity representing energy. The Rydberg levels belonging to these two interacting channels lie at the intersections between a family of curves represented by Eqs. (2) and (3). In other words, these three parameters, $\mu_\alpha, \alpha=1$, 2, and θ, together with the ion-core fine-structure splitting $\Delta I = I_2 - I_1$, *completely* determine the properties of the two mutually perturbing Rydberg series.

In the autoionization region, $I_1 < E < I_2$, one of the channels is *open,* whereas the other is *closed.* One simply replaces the quantum defect μ by the phase shift τ for the open channel in Eq. (3).[5] In other words, the behavior of an eigenphase shift near resonance in the autoionization region is described by the same expression in Eq. (3). The derivative $d\tau/dE$, which measures the delay time of the autoionization resonance due to the open-channel interaction with the closed channel, is then proportional to the channel interaction strength $d\tau/d\nu_2$ which in turn is equal to the slope of the quantum-defect plot (μ,ν_2).[1] Therefore, the same basic quantum-defect parameters characterize the autoionization resonances.

III. CALCULATION OF EIGENCHANNEL QUANTUM-DEFECT PARAMETERS

In this section we aim at establishing the connection between the eigenchannel quantum-defect theory and the configuration-mixing method. This connection allows one to use well-established Hartree-Fock (HF) computer codes[10] to calculate eigenchannel quantum-defect parameters. Eigenvalues and eigenvectors of the eigenchannels and of the time-delay matrices are expressed in terms of quantum-defect parameters. Thus, the energy positions of excited Rydberg levels as well as autoionization resonance can be predicted provided the basic quantum-defect parameters are known.

We first diagonalize the Hamiltonian including electrostatic and spin-orbit interactions of the configuration p^4s for $J=\frac{1}{2}$ and $\frac{3}{2}$ in the basis of LS coupling. The eigenvalues and eigenvectors are

$$E_{1,2} = (E_{\rm av} - \tfrac{3}{25}F^2 + \tfrac{1}{6}G^1 - \tfrac{3}{4}\zeta_{3p}) \pm [(\tfrac{1}{2}G^1 + \tfrac{1}{12}\zeta_{3p})^2 + \tfrac{1}{18}\zeta_{3p}^2]^{1/2} , \tag{4}$$

$$\theta_{\bar{\alpha}\alpha} = \tfrac{1}{2}\arctan\left[\frac{-(\sqrt{2}/3)(\zeta_{3p}/G^1)}{1+\frac{1}{6}(\zeta_{3p}/G^1)}\right] \quad \text{for } J=\tfrac{1}{2} , \tag{5}$$

and

$$E_{1,2} = (E_{\rm av} - \tfrac{3}{25}F^2 + \tfrac{1}{6}G^1) \pm [(\tfrac{1}{2}G^1 + \tfrac{1}{3}\zeta_{3p})^2 + \tfrac{5}{36}\zeta_{3p}^2]^{1/2} , \tag{6}$$

$$\theta_{\bar{\alpha}\alpha} = \tfrac{1}{2}\arctan\left[\frac{-\sqrt{5}/3(\zeta_{3p}/G^1)}{1+\frac{2}{3}(\zeta_{3p}/G^1)}\right] \quad \text{for } J=\tfrac{3}{2} , \tag{7}$$

where $E_{\rm av}$ is the average energy of the p^4s configuration, F^2 and G^1 are Slater integrals, and ζ_{3p} is the spin-orbit coupling parameter. The mixing angle $\theta_{\bar{\alpha}\alpha}$ represents the orthogonal transformation matrix $V_{\bar{\alpha}\alpha}$ which diagonalizes the Hamiltonian from the LS coupling, $\bar{\alpha}$, basis into the α basis. The diagonalization is carried out at each energy level E_n.

On the other hand, the eigen quantum defect μ_α and channel-mixing angle θ are the eigenvalues and eigenvectors of reaction matrix $\underline{R}$:

TABLE II. EQDT parameters.

J	Channel	μ_α	$\theta_{\bar{\alpha}}$	$\theta_{\bar{\alpha}\alpha}$	$\theta=\theta_{\bar{\alpha}}+\theta_{\bar{\alpha}\alpha}$	$\lvert D_\alpha \rvert$
$\frac{1}{2}$	$3p^4(^3P_1)ns$	0.10				0.0645
			35.26°	0.68°	35.94°	
$\frac{1}{2}$	$3p^4(^3P_0)ns'$	0.09				0.3145
$\frac{3}{2}$	$3p^4(^3P_2)ns$	0.095				0.138
			24.09°	1.096°	25.19°	
$\frac{3}{2}$	$3p^4(^3P_1)ns'$	0.085				1.058
$\frac{5}{2}$	$3p^4(^3P_2)ns$	0.12	0	0	0	

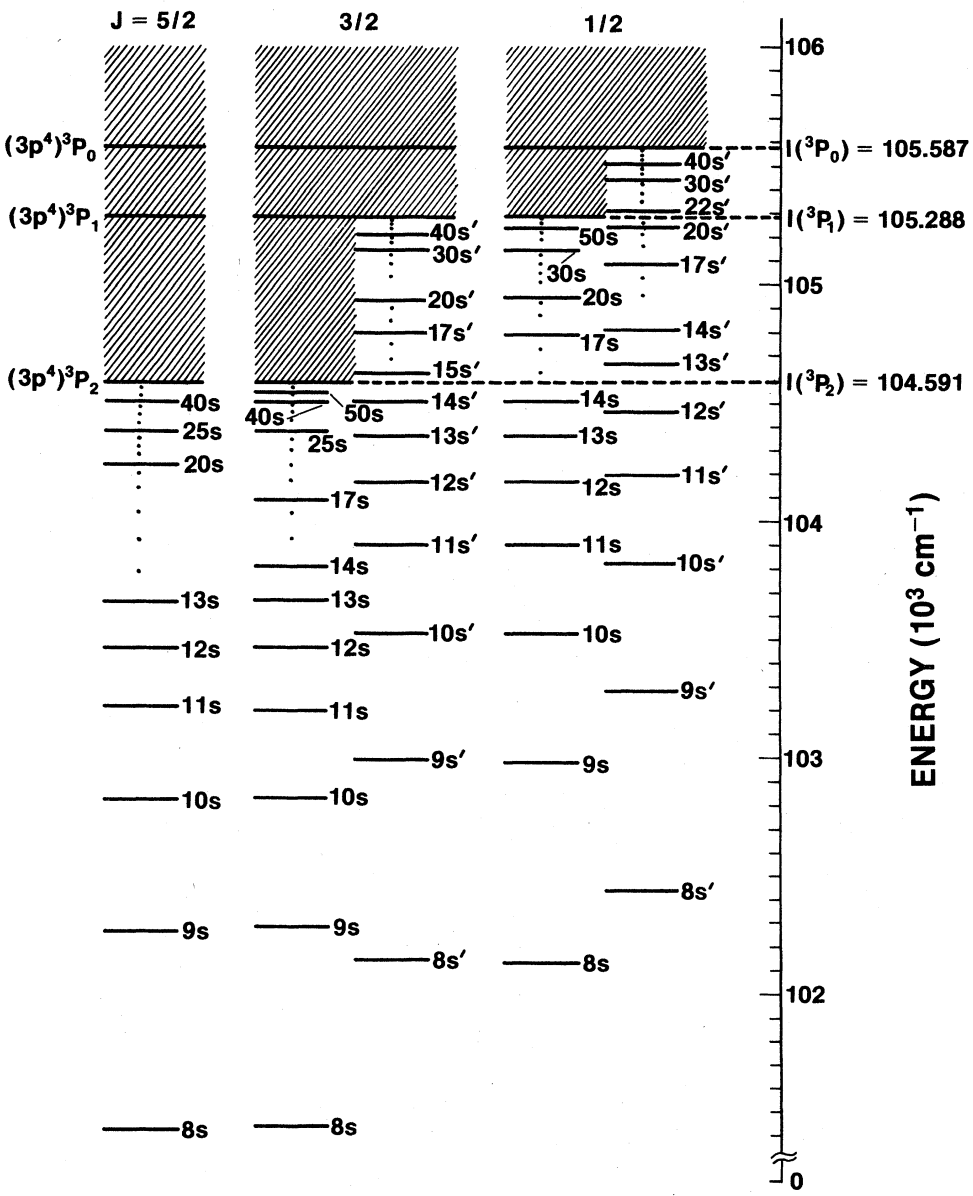

FIG. 1. The theoretical level diagram for all five channels.

$$\delta_{\alpha\beta}\tan(\pi\mu_\alpha)=\sum_{i,j}(U^{-1})_{\alpha i}R_{ij}U_{j\beta}\ . \tag{8}$$

These parameters measure the short-range dynamical interactions including electrostatic electron correlations and spin-orbit interactions and are treated as *independent* functions of energy. In the dissociation channel i, the electron is attracted to the ion core by the small long-range Coulomb field and the fine structure of the ion core stands out. Therefore, electron's angular momentum coupling with the core is better described in terms of the jj coupling scheme. In the reactive channel $\bar{\alpha}$, the electron is coupled strongly to the ion core by the electrostatic interactions; thus the LS-coupling scheme is a better description. However, the eigenchannel α is not purely LS coupled because of the spin-orbit interactions. The transformation from i-channel jj coupling to the eigenchannel α can be carried out by an intermediate transformation $V_{\bar{\alpha}\alpha}$,

$$U_{i\alpha}=\sum_{\bar{\alpha}}U_{i\bar{\alpha}}V_{\bar{\alpha}\alpha}\ , \tag{9}$$

where $V_{\bar{\alpha}\alpha}$ is an orthogonal matrix that diagonalizes the Hamiltonian. The matrix $U_{i\bar{\alpha}}$ is the jj-LS orthogonal transformation and is known analytically. For a 2×2 matrix, the relation (9) can be expressed in terms of mixing angles,

$$\theta=\theta_{\bar{\alpha}}+\theta_{\bar{\alpha}\alpha}\ , \tag{10}$$

where θ is related to a 2×2 orthogonal matrix by

$$U_{i\alpha}=\begin{bmatrix}\cos\theta & \sin\theta\\ -\sin\theta & \cos\theta\end{bmatrix}\ . \tag{11}$$

For $J=\frac{1}{2}$, $\theta_{\bar{\alpha}}=35.26°$ and for $J=\frac{3}{2}$, $\theta_{\bar{\alpha}}=24.09°$. According to Eq. (1), the eigen quantum defect μ_α can be expressed in terms of the eigenvalues of the Hamiltonian in Eq. (4) or (6) as

$$\Delta_{\alpha\beta}=\mu_\alpha-\mu_\beta=\Delta\nu_1=\nu_1^3\Delta E$$
$$=\nu_1^3G^1(1+\tfrac{1}{3}x+\tfrac{1}{4}x^2)^{1/2}\qquad \text{for } J=\tfrac{1}{2} \tag{12a}$$

and

$$\Delta_{\alpha\beta}=\mu_\alpha-\mu_\beta=\Delta\nu_1=\nu_1^3\Delta E$$
$$=\nu_1^3G^1(1+\tfrac{1}{3}x+\tfrac{1}{4}x^2)^{1/2}\qquad \text{for } J=\tfrac{3}{2}\ , \tag{12b}$$

where x is the ratio of spin-orbit energy ζ_{3p} to the Slater exchange integral G^1. The expression $\nu_1^3G^1$ is *independent* of the effective quantum number, namely, energy. The calculated values of ζ_{3p}, G^1, and $\nu_1^3G^1$ using the HF program[10] are listed in Table I. As expected, $\nu_1^3G^1$ is nearly independent of ν_1 or of energy levels. We take the mean value of $\nu_1^3G^1$ for ^4P to be 13 317.46 cm^{-1} and ^2P to be 11 630.17 cm^{-1}. We use the weighted mean value of $\nu_1^3G^1$ for ^4P and ^2P as the Slater exchange integral G^1 in Eqs. (12a) and (12b) to evaluate the eigen quantum defect parameters from Eqs. (5), (7), and (12). For $J=\frac{1}{2}$, the mixing angle $\theta_{\bar{\alpha}\alpha}=0.68°$ and $\theta=\theta_{\bar{\alpha}}+\theta_{\bar{\alpha}\alpha}=35.94°$ and $\Delta_{\alpha\beta}=\mu_\alpha-\mu_\beta=0.0105$. For $J=\frac{3}{2}$, the mixing angle $\theta_{\bar{\alpha}\alpha}=1.096°$ and $\theta=25.19°$ and $\Delta_{\alpha\beta}=0.0093$. These results are shown in Table II. Note that the difference $\Delta_{\alpha\beta}$ of the eigen quantum defect is independent of the total energy $E_{\rm av}$. Thus, it is a more meaningful quantity to be evaluated in terms of the HF program which takes care of no configuration interactions. The eigen quantum defect μ_α is obtained by the normalization to the lowest Rydberg energy levels. The resulting quantum-defect parameters μ_α and θ for $J=\frac{1}{2}$, $\frac{3}{2}$, and $\frac{5}{2}$ are listed in Table II.

IV. RESULTS

The Rydberg discrete levels and autoionization resonance positions for $p^4(^3P)ns$, $J=\frac{1}{2}$, $\frac{3}{2}$, and $\frac{5}{2}$ channels, are calculated from Eqs. (1)—(3) with quantum-defect parameters obtained in Table II as input. The values of ionization limits, $p^4(^3P_{2,1,0})$, of the chlorine atom are taken from Ref. 3. The calculated Rydberg energy levels and the predicted autoionization resonance positions are listed in Table III. The energy-level diagram for all five channels is plotted in Fig. 1. The Lu-Fano plots for $J=\frac{1}{2}$ and $\frac{3}{2}$ channels are shown in Fig. 2(a). The experimental data are also listed in Table III for comparison. The agreement for energy levels with $n>4$ is excellent. For autoionization resonances, there are no measurements suitable for comparison.

The oscillator strength for the nth state is written as[15]

$$f_n=2(E_n-E_0)\left|\sum_{\alpha=1}^{2}D_\alpha A_\alpha^{(n)}\right|^2\Big/N_n^2\ , \tag{13a}$$

where D_α ($\alpha=1,2$) are the dipole matrix elements. The normalization factor N_n is given by

$$N_n^2=\left[\nu_{1,n}^3+\nu_{2,n}^3\left[\frac{d(-\nu_1)}{d\nu_2}\right]_n\right]\left[\frac{d(-\nu_1)}{d\nu_2}\right]_n^{-1}\ , \tag{13b}$$

where

$$\frac{d(-\nu_1)}{d\nu_2}=\tan^2\theta\frac{\sin^2[\pi(\nu_1+\mu_2)]}{\sin^2[\pi(\nu_2+\mu_2)]} \tag{13c}$$

is the slope of $\mu(\nu_2)$ curves in Fig. 2(a). The mixing coefficients A_α are given by

$$A_1(\nu_2)=\frac{\sin[\pi(\nu_2+\mu_2)]}{\sin\theta\sin[\pi(\mu_1-\mu_2)]}\ ,$$
$$A_2(\nu_2)=\frac{\sin[\pi(\nu_2+\mu_1)]}{\cos\theta\sin[\pi(\mu_1-\mu_2)]}\ . \tag{13d}$$

Experimental oscillator strength data for the $4s$ manifold[16] are used as input to evaluate the dipole matrix elements D_α. The fitted results are listed in Table II.

For a two-channel case, the density of the oscillator strength of an autoionization resonance can be written[15] as

$$df(\nu_2)/dE=2(E-E_0)I_0\sin^2[\pi(\nu_2-\nu_0)](d\tau/d\nu_2)\ , \tag{14a}$$

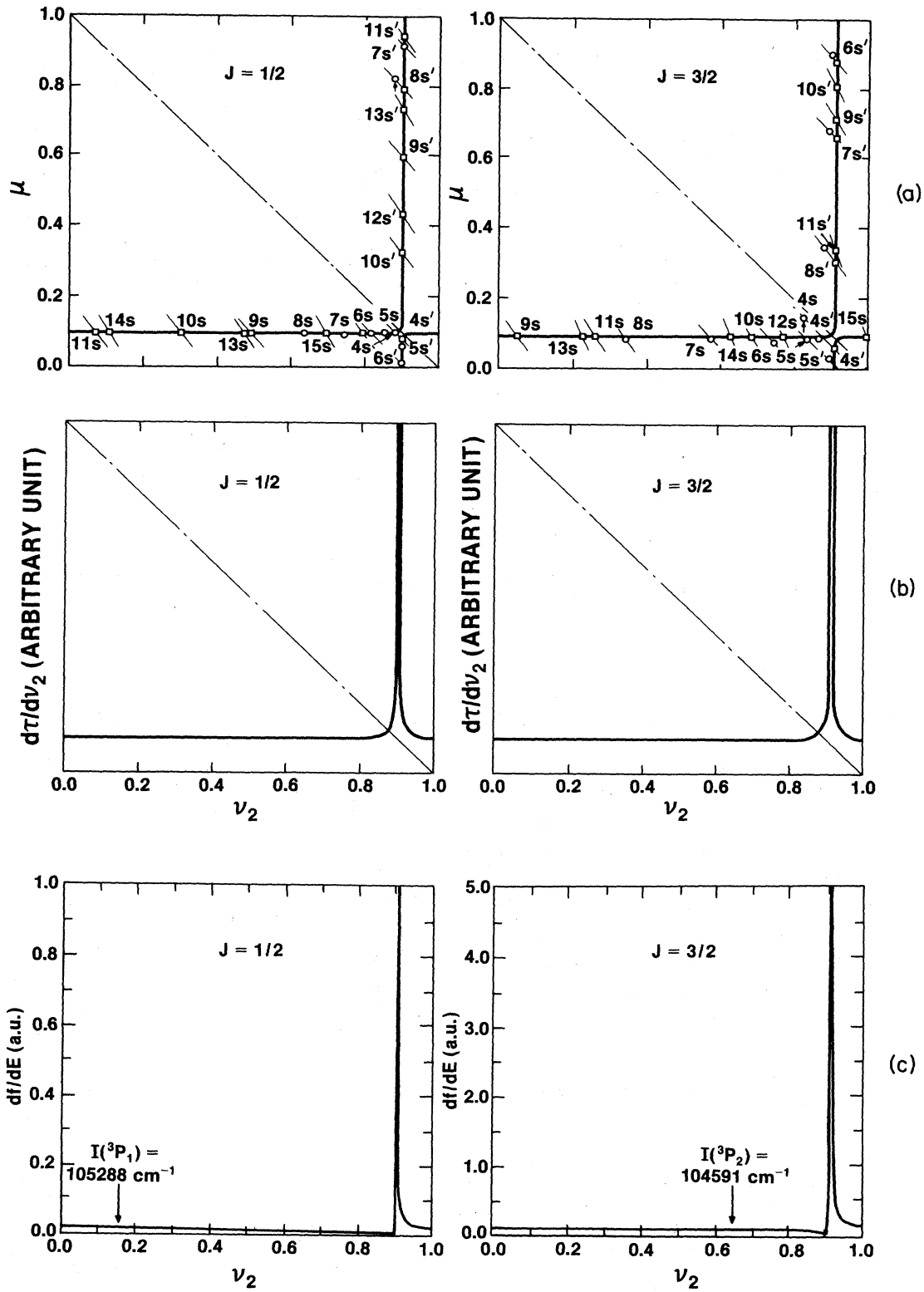

FIG. 2. (a) The Lu-Fano plots for $J=\frac{1}{2}$ and $\frac{3}{2}$ channels. Open circles represent the experimental level positions from Ref. 3. Open squares represent the theoretical level positions. The function $-\nu(\nu_2)$ defined by Eq. (2) is represented by thin lines. (b) Time delay $d\tau/d\nu_2$ as a function of ν_2, for $J=\frac{1}{2}$ and $\frac{3}{2}$. (c) Autoionization resonance profile, for $J=\frac{1}{2}$ and $\frac{3}{2}$.

TABLE III. (a) The discrete levels and the autoionization resonance positions for $J=\frac{1}{2}$ [for $J=\frac{1}{2}$, $I_1(^3P_1)=105\,288$ cm^{-1} and $I_2(^3P_0)=105\,587$ cm^{-1}]. (b) The discrete levels and the autoionization resonance positions for $J=\frac{3}{2}$ [for $J=\frac{3}{2}$, $I_1(^3P_2)=104\,591$ cm^{-1} and $I_2(^3P_1)=105\,288$ cm^{-1}]. (c) The discrete levels for $J=\frac{5}{2}$ [for $J=\frac{5}{2}$, $I(^3P_2)=104\,591$ cm^{-1}].

	ν_1	ν_2	E_{theor} (cm^{-1})	E_{expt}[a] (cm^{-1})		ν_1	ν_2	E_{theor} (cm^{-1})	E_{expt}[a] (cm^{-1})
				(a)					
$3p^4(^3P)4s$	1.902	1.894	74 942.93	72 827.038	$3p^4(^3P)4s'$	1.925	1.916	75 688.65	74 865.667
$3p^4(^3P)5s$	2.903	2.870	92 263.10	92 151.38	$3p^4(^3P)5s'$	2.941	2.907	92 603.32	92 602.70
$3p^4(^3P)6s$	3.903	3.825	98 084.92	98 100.34	$3p^4(^3P)6s'$	3.991	3.907	98 397.03	98 390.74
$3p^4(^3P)7s$	4.903	4.750	100 723.76	100 737.65	$3p^4(^3P)7s'$	5.076	4.906	101 028.50	101 039.413
$3p^4(^3P)8s$	5.903	5.641	102 139.19	102 138.11	$3p^4(^3P)8s'$	6.209	5.906	102 441.2	102 411.57
$3p^4(^3P)9s$	6.903	6.495	102 985.4		$3p^4(^3P)9s'$	7.404	6.906	103 286.25	
$3p^4(^3P)10s$	7.903	7.306	103 531.24		$3p^4(^3P)10s'$	8.680	7.906	103 831.46	
$3p^4(^3P)11s$	8.903	8.074	103 903.73		$3p^4(^3P)11s'$	10.059	8.906	104 203.55	
$3p^4(^3P)12s$	9.903	8.797	104 169.09		$3p^4(^3P)12'$	11.574	9.906	104 468.76	
$3p^4(^3P)13s$	10.903	9.476	104 364.96		$3p^4(^3P)13s'$	13.266	10.906	104 664.43	
$3p^4(^3P)14s$	11.903	10.110	104 513.55		$3p^4(^3P)14s'$	15.198	11.906	104 812.89	
$3p^4(^3P)17s$	14.903	11.763	104 793.94		$3p^4(^3P)17s'$	23.730	14.906	105 093.13	
$3p^4(^3P)20s$	17.904	13.081	104 945.65		$3p^4(^3P)20s'$	49.940	17.906	105 244.75	
$3p^4(^3P)22s$	19.904	13.803	105 011.01		$3p^4(^3P)22s'$		19.906	105 310.06	
$3p^4(^3P)25s$	22.903	14.695	105 078.81		$3p^4(^3P)25s'$		22.906	105 377.86	
$3p^4(^3P)30s$	27.903	15.793	105 147.06		$3p^4(^3P)30s'$		27.906	105 446.09	
$3p^4(^3P)40s$	37.904	17.098	105 211.62		$3p^4(^3P)40s'$		37.906	105 510.63	
$3p^4(^3P)50s$	47.904	17.788	105 240.18		$3p^4(^3P)50s'$		47.906	105 539.19	
				(b)					
$3p^4(^3P)4s$	1.907	1.885	74 402.78	72 488.568	$3p^4(^3P)4s'$	1.937	1.914	75 333.39	74 225.846
$3p^4(^3P)4s$	2.907	2.832	91 601.78	91 680.99	$3p^4(^3P)5s'$	2.995	2.913	92 355.97	92 140.127
$3p^4(^3P)6s$	3.907	3.730	97 401.17	97 480.664	$3p^4(^3P)6s'$	4.118	3.913	98 121.16	98 044.980
$3p^4(^3P)7s$	4.907	4.570	100 033.23	100 050.736	$3p^4(^3P)7s'$	5.339	4.913	100 741.74	100 704.23
$3p^4(^3P)8s$	5.907	5.344	101 445.86	101 460.16	$3p^4(^3P)8s'$	6.704	5.913	102 149.43	102 108.84
$3p^4(^3P)9s$	6.907	6.051	102 290.77		$3p^4(^3P)9s'$	8.284	6.913	102 991.78	
$3p^4(^3P)10s$	7.907	6.689	102 835.70		$3p^4(^3P)10s'$	10.196	7.913	103 535.47	
$3p^4(^3P)11s$	8.907	7.263	103 207.75		$3p^4(^3P)11s'$	12.663	8.913	103 906.66	
$3p^4(^3P)12s$	9.907	7.775	103 472.88		$3p^4(^3P)12s'$	16.170	9.913	104 171.29	
$3p^4(^3P)13s$	10.907	8.232	103 668.53		$3p^4(^3P)13s'$	22.112	10.913	104 366.57	
$3p^4(^3P)14s$	11.907	8.637	103 816.96		$3p^4(^3P)14s'$	37.941	11.913	104 514.77	
$3p^4(^3P)15s$	12.907	8.997	103 932.27		$3p^4(^3P)15s'$		12.913	104 629.90	
$3p^4(^3P)17s$	14.907	9.599	104 097.16		$3p^4(^3P)17s'$		14.913	104 793.92	
$3p^4(^3P)20s$	17.907	10.276	104 248.77		$3p^4(^3P)20s'$		17.913	104 946.01	
$3p^4(^3P)25s$	22.907	11.005	104 381.87		$3p^4(^3P)25s'$		22.913	105 078.98	
$3p^4(^3P)30s$	27.907	11.444	104 450.09		$3p^4(^3P)30s'$		27.913	105 147.16	
$3p^4(^3P)40s$	37.907	11.912	104 514.64		$3p^4(^3P)40s'$		37.913	105 211.66	
$3p^4(^3P)50s$	47.907	12.138	104 543.19		$3p^4(^3P)50s'$		47.913	105 240.20	

TABLE III. (*Continued*).

	ν_1	E_{theor} (cm^{-1})	E_{expt}[a] (cm^{-1})	(c)	ν_1	E_{theor} (cm^{-1})	E_{expt}[a] (cm^{-1})
$3p^4(^3P)4s$	1.88	73 543.13	71 958.363	$3p^4(^3P)11s$	8.88	103 199.37	
$3p^4(^3P)5s$	2.88	91 360.90	91 343.50	$3p^4(^3P)12s$	9.88	103 466.81	
$3p^4(^3P)6s$	3.88	97 301.70	97 237.723	$3p^4(^3P)13s$	10.88	103 663.98	
$3p^4(^3P)7s$	4.88	99 983.0	99 988.501	$3p^4(^3P)14s$	11.88	103 813.48	
$3p^4(^3P)8s$	5.88	101 417.10	101 426.204	$3p^4(^3P)20s$	17.88	104 247.75	
$3p^4(^3P)9s$	6.88	102 272.70		$3p^4(^3P)25s$	22.88	104 381.38	
$3p^4(^3P)10s$	7.88	102 823.82		$3p^4(^3P)40s$	37.88	104 514.52	

[a]Experimental levels from Ref. 3.

where ν_0 represents the value of ν_2 at which df/dE vanishes. Quantities ν_0 and I_0 are defined by

$$\frac{\sin[\pi(\nu_0+\mu_2)]}{\sin[\pi(\nu_0+\mu_1)]}=-\frac{D_2}{D_1}\tan\theta \tag{14b}$$

and

$$I_0=D_1^2\cos^2\theta+D_2^2\sin^2\theta +2D_1D_2\sin\theta\cos\theta\cos[\pi(\mu_1-\mu_2)]\ . \tag{14c}$$

The value of df/dE of the autoionization resonances as a function of ν_2 is plotted in Fig. 2(c) for $J=\frac{1}{2}$ and $\frac{3}{2}$ channels. The positions of the resonances are listed in Table III. The resonance profile shows an asymmetric Fano line shape with a zero-intensity points, e.g., at $E=105\,309.9\ \text{cm}^{-1}$ for the first resonance located at $E=105\,310.1\ \text{cm}^{-1}$ above the ionization limit $p^4(^3P_1)$, $J=\frac{1}{2}$. The half-width at full maximum is $\sim 1\ \text{cm}^{-1}$. However, the density of the oscillator strength for $J=\frac{3}{2}$ is by one order of magnitude larger than that of $J=\frac{1}{2}$. The corresponding time delay, which is proportional to the slope $d\tau/d\nu_2$, is plotted in Fig. 2(b).

V. DISCUSSION

Properties of Rydberg spectra of $p^4(^3P)ns$ channels, such as energy levels, autoionization resonance positions, and time delay, are predicted from the calculated eigenquantum-defect μ_α and the channel-mixing angle θ. The results indicate very weak channel interactions between the pairs of channels. The s-d interaction, as well as the effect due to the $3s3p^6$ interloper, are negligible.

Experimental oscillator strengths for the $4s$ manifold were used to infer the autoionization resonance profile. The dipole matrix element D_α is determined accordingly. An asymmetric Fano profile for a very narrow autoionization resonance with width $\sim 1\ \text{cm}^{-1}$ is predicted. Experimental investigation for these resonances would be very challenging, since the chlorine atom, like most open-shell atoms, does not have a ground state with total angular momentum $J=0$. It requires high resolution to separate levels and resonances with different J' in the final states, in particular for continuum spectra.

A natural extension of the present method is to calculate eigenchannel quantum-defect parameters as functions of effective nuclear charge z so that the spectra of the isoelectronic ions can be analyzed.[17] Calculation of $3p^4(^3P)nd$ Rydberg spectra of the chlorine atom using the present method is underway.

ACKNOWLEDGMENTS

This work has been performed under the auspices of the U.S. Department of Energy. One of us (Z.W.W.) was a Visiting Foreign Scholar at Argonne National Laboratory. We are indebted to Dr. K.-N. Huang and Dr. K. T. Cheng for assistance in computations.

*Permanent address: Institute of Atomic and Molecular Physics, Jilin University, Changchun, People's Republic of China.

†Present address: Graduate School, Academia Sinica, Beijing, People's Republic of China.

[1]Z.-w. Wang and K. T. Lu, preceding paper [Phys. Rev. A **31**, 1515 (1985)].

[2]B. Ruščić and J. Berkowitz, Phys. Rev. Lett. **50**, 675 (1983).

[3]L. J. Radziemski, Jr. and V. Kaufman, J. Opt. Soc. Am. **59**, 424 (1969).

[4]K. T. Lu and M. Mansfield, in *Electron and Photon Interaction with Atoms,* edited by H. Kleinpoppen and M. R. C. McDowell (Plenum, New York, 1975), p. 627.

[5]K. T. Lu, in *Photophysics and Photochemistry in Vacuum Ultraviolet,* edited by S. P. McGlynn, G. L. Findley, and R. H. Huebner (Reidel, Dortrecht, Holland, 1983).

[6]U. Fano, J. Opt. Soc. Am. **65**, 979 (1975).

[7]C. M. Lee, Phys. Rev. A **10**, 584 (1974).

[8]C. M. Lee and W. R. Johnson, Phys. Rev. A **22**, 979 (1980).

[9]W. R. Johnson, K. T. Cheng, K.-N. Huang, and M. LeDourneuf, Phys. Rev. A **22**, 989 (1980).

[10]C. Froese Fischer, Comput. Phys. Commun. **14**, 145 (1978).

[11]A. C. Wahl and G. Das, Adv. Quantum Chem. **5**, 261 (1970).

[12]A. F. Starace and L. Armstrong, Jr., Phys. Rev. A **13**, 1850 (1976).

[13]M. Lamoureux and F. Combet-Farnoux, J. Phys. (Paris) **40**, 545 (1979).

[14]E. R. Brown, S. L. Carter, and H. P. Kelly, Phys. Rev. A **21**, 1237 (1980).

[15]K. T. Lu, Proc. R. Soc. London, Ser. A **353**, 431 (1977).

[16]W. L. Wiese, F. T. Smith, and Miles, *Atomic Transition Probabilities—Sodium Through Calcium,* Natl. Bur. Stand. Ref. Data Ser., Natl. Bur. Stand. (U.S.) Circ. No. 22 (U.S. GPO, Washington, D.C., 1969), Vol. II, p. 159.

[17]K.-N. Huang, Y.-K. Kim, K. T. Cheng, and J. P. Desclaux, At. Data Nucl. Data Tables **28**, 355 (1983).